
NEURO-SYMBOLIC CONTROL WITH LARGE LANGUAGE MODELS FOR LANGUAGE-GUIDED SPATIAL TASKS

Momina Liaqat Ali*

Department of Computer Science,
Middle Tennessee State University,
Murfreesboro, TN 37130, USA.
ma2mp@mtmail.mtsu.edu

Muhammad Abid

Department of Mechanical and Aerospace Engineering,
University of Tennessee,
Knoxville, TN 37996, USA.
mabid@vols.utk.edu

ABSTRACT

Although large language models (LLMs) have recently become effective tools for language-conditioned control in embodied systems, instability, slow convergence, and hallucinated actions continue to limit their direct application to continuous control. A modular neuro-symbolic control framework that clearly distinguishes between low-level motion execution and high-level semantic reasoning is proposed in this work. While a lightweight neural delta controller performs bounded, incremental actions in continuous space, a locally deployed LLM interprets symbolic tasks. We assess the suggested method in a planar manipulation setting with spatial relations between objects specified by language. Numerous tasks and local language models, such as Mistral, Phi, and LLaMA-3.2, are used in extensive experiments to compare LLM-only control, neural-only control, and the suggested LLM+DL framework. In comparison to LLM-only baselines, the results show that the neuro-symbolic integration consistently increases both success rate and efficiency, achieving average step reductions exceeding 70% and speedups of up to $8.83 \times$ while remaining robust to language model quality. The suggested framework enhances interpretability, stability, and generalization without any need of reinforcement learning or costly rollouts by controlling the LLM to symbolic outputs and allocating uninterpreted execution to a neural controller trained on artificial geometric data. These outputs show empirically that neuro-symbolic decomposition offers a scalable and principled way to integrate language understanding with ongoing control, this approach promotes the creation of dependable and effective language-guided embodied systems.

Keywords Neuro-Symbolic Control · LLMs · Language-Guided Robotics · Closed-Loop Control · Robotics · Deep Learning · Autonomous Systems

1 Introduction

Recent developments in large language models (LLMs) have shown their exceptional capacity for high-level decision-making, reasoning, and instruction following [2, 1]. These kinds of models are being studied extensively as cognitive engines for robotics and control systems, where they are employed to create the different tasks and plans, choose actions in complex environments, and interpret natural language instructions. However, when used in closed-loop control settings, LLMs show basic limitations despite their expressive power [3]. Particularly, LLM-only control policies typically suffer from hallucinated actions, poor sample efficiency, lack of convergence guarantees, and brittle behavior under feedback, which makes them unreliable for precise spatial manipulation and continuous control tasks [4, 5]. As illustrated in Fig. 1, directly using large language models for continuous control leads to unstable behavior, motivating the proposed neuro-symbolic decomposition.

In parallel, learning-based controllers such as deep neural networks have achieved strong performance in low-level control and perception tasks, benefiting from fast inference, smooth action outputs, and stability under feedback. However, these models typically lack symbolic reasoning and struggle to generalize across tasks without retraining [6].

*Corresponding author. Email: ma2mp@mtmail.mtsu.edu

Purely neural controllers are therefore limited in their ability to handle task-level abstraction, compositional instructions, or symbolic relational reasoning such as spatial constraints (e.g., *left of*, *right of*, *above*, *below*).

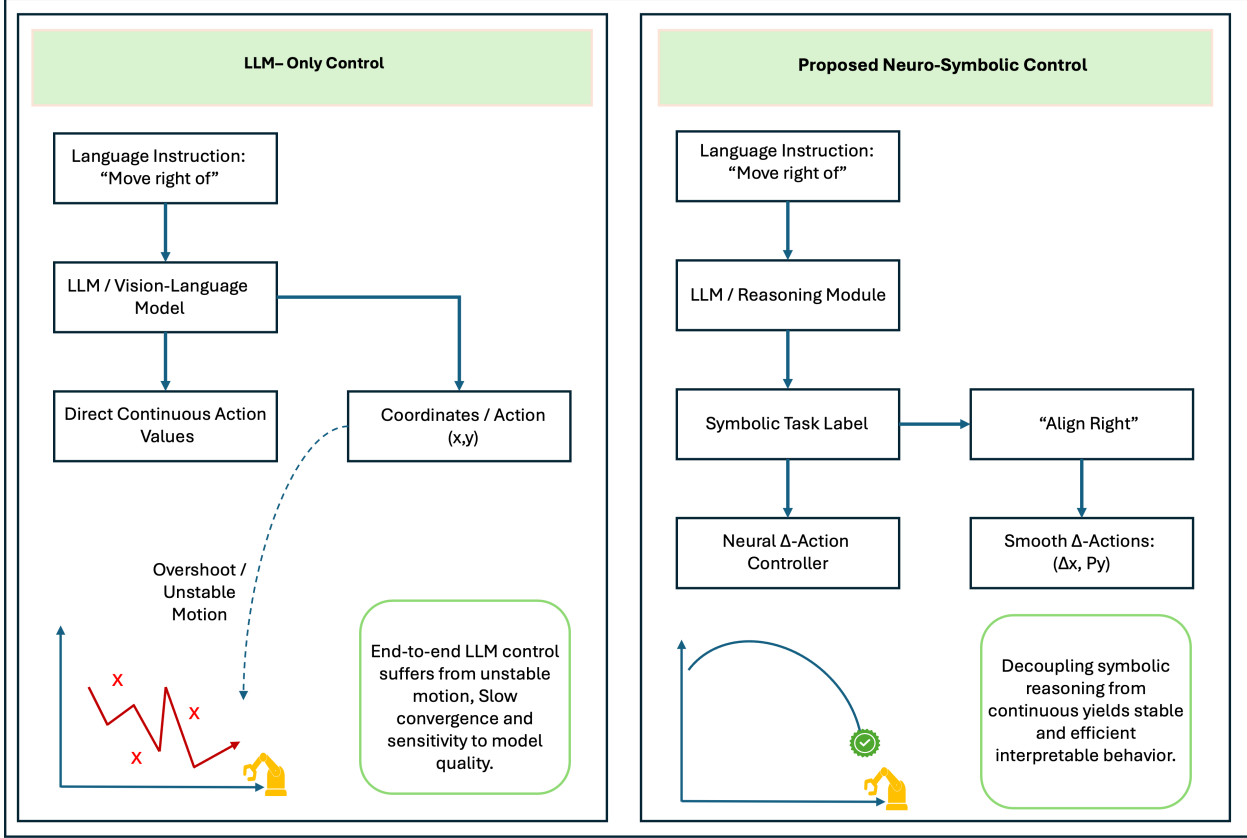


Figure 1: Motivation for neuro-symbolic control. End-to-end LLM-based control directly predicts continuous actions, leading to unstable motion and slow convergence. Our approach decouples symbolic reasoning from continuous execution, combining LLM-based semantic understanding with a neural delta controller for stable and efficient closed-loop control.

This dichotomy has motivated growing interest in neuro-symbolic control, which seeks to combine the complementary strengths of symbolic reasoning systems and neural function approximators. In this paradigm, symbolic components provide task-level reasoning and interpretability, while neural modules handle continuous control and execution. While prior work has explored hybrid approaches using classical symbolic planners or handcrafted logic modules [7], the emergence of LLMs offers a new opportunity: using language models as flexible, general-purpose symbolic planners that can reason over tasks, goals, and constraints expressed in natural language.

Nevertheless, directly deploying LLMs as action generators in control loops still remains the problematic [8]. LLM outputs are fundamentally stochastic, sensitive to prompt phrasing, and also not optimized for numerical precision [9]. These type issues become particularly pronounced in spatial control tasks, where the small positional errors can lead to task failure or also towards slow convergence. In term of the result in this scenario, recent studies have highlighted the need for structured interfaces and also the auxiliary control mechanisms to ground LLM reasoning in stable, low-level execution [10].

In the current research work, we propose a neuro-symbolic closed-loop control framework that precisely integrates local large language models with a lightweight type of neural delta controller. So, the LLM is responsible for high-level symbolic reasoning, task interpretation, and also for the goal selection, while the neural controller executes fine-grained corrective actions that ensure fast and stable convergence. By empowering the numerical control to the neural module and restricting the LLM to structured symbolic outputs, the proposed framework clearly mitigates hallucinations, reduces action variance, and significantly improves the sample efficiency.

A fundamental aspect of our proposed approach is the use of locally hosted LLMs, including Mistral, Phi, and LLaMA-3.2. Unlike cloud-based proprietary models, local LLMs facilitate reproducibility, low-latency inference,

privacy preservation, and deployment on edge or also resource-constrained systems. Local models, although they are often smaller and less robust than large proprietary counterparts, make them one of the best testbeds for evaluating whether neuro-symbolic integration can compensate for limited model capacity. Our results clearly demonstrate that the proposed hybrid framework consistently improves performance across all evaluated local LLMs, also indicating that the improvements arise from architectural synergy rather than the model scale alone.

We evaluate our method on a suite of spatial reasoning and control tasks in a simulated 2D environment, including relational goals such as *right of*, *left of*, *above*, and *below*. We compare three settings: LLM-only control, deep learning (DL)-only control, and the proposed LLM+DL hybrid. Extensive experiments show that the hybrid approach achieves substantially higher success rates, reduces the number of control steps by up to an order of magnitude, and yields significant speedups over LLM-only baselines. These improvements are consistent across many different types of LLM architectures and tasks, clearly highlighting the robustness and generality of the proposed framework.

Here are the main and clear contributions of this paper as follows:

- We introduce a neuro-symbolic closed-loop control architecture that combines LLM-based symbolic reasoning along neural delta controller for stable execution.
- We provide a rigorous evaluation of the local LLMs (including Mistral, Phi, and LLaMA-3.2) in spatial control tasks, those highlighting their limitations in isolation and their strengths when integrated with neural control.
- We show the major improvements in success rate, convergence speed, and also efficiency using the proposed hybrid framework, supported by a comprehensive quantitative analysis and ablation studies.
- We release a reproducible experimental pipeline and evaluation framework that facilitates further research on neuro-symbolic control with local LLMs.

2 Related Work

This work intersects several active research areas, including large language models for control, neuro-symbolic reasoning, hybrid planning and control architectures, and learning-based spatial reasoning. We review the most relevant literature and highlight how our approach differs from prior work.

2.1 Large Language Models for Planning and Control

Large language models have recently been explored as high-level planners and controllers for robotic systems due to their strong reasoning and instruction-following capabilities [11, 12]. Traditional methods demonstrated that LLMs can generate action sequences, code, or symbolic plans from natural-language task descriptions, which enables them to have flexible task specification and zero-shot generalization [13]. Common examples include planning for language-driven frameworks that translate instructions into executable programs or symbolic action graphs.

Several landmark studies have applied LLMs directly to robotic control loops. SayCan [14] demonstrated that combining LLM-based task planning with learned affordance functions enables robots to execute complex, multi-step instructions in real kitchen environments. PaLM-E [15] extended this paradigm by incorporating multimodal sensor inputs directly into the language model, enabling end-to-end embodied reasoning across manipulation and navigation tasks. Code-as-Policies [16] showed that code-writing LLMs can generate executable robot policies that exhibit spatial-geometric reasoning and generalize to new instructions without additional training.

While promising, LLM-only approaches often suffer from instability, hallucinated actions, and slow convergence due to the lack of grounding in physical dynamics [17]. According to empirical investigations, LLM-only controllers perform poorly on tasks those requiring exact numerical reasoning or spatial accuracy [18], show considerable variance between trials, and are sensitive to prompt phrasing. In most recent work, that has attempted to mitigate these issues through prompt engineering, structured outputs (e.g., JSON schemas), or iterative replanning [19]. However, such methodologies do not essentially address the mismatch among the discrete language reasoning and continuous control execution. But our work explicitly separates symbolic reasoning and numerical control, using the LLM only for high-level task with interpretation while delegating execution to a neural controller trained for stability and precision.

2.2 Neuro-Symbolic and Hybrid Reasoning Systems

Neuro-symbolic AI aims to combine the comprehensibility and also the compositionality of symbolic reasoning with the scalability and robustness of neural networks [20, 21]. Classical methods especially integrate logic-based systems, rule engines, or symbolic planners with neural perception or control modules [22]. These type of methods have been applied in domains such as visual reasoning, program induction, and task planning [23].

In the robotics field, hybrid symbolic-neural architectures often employ symbolic task planners (e.g., STRIPS, PDDL-based planners) coupled with some low-level controllers learned via reinforcement learning or also supervised learning [24]. While effective, these kinds of approaches typically depend on the handcrafted symbolic representations and domain-specific planners, limiting flexibility and scalability.

In the recent advances, they propose replacing classical symbolic planners with LLMs, leveraging their ability to reason over diverse tasks without explicit domain modeling [25]. However, many existing LLM-based neuro-symbolic systems specially focus on open-loop planning or single-shot decision-making rather than closed-loop control [26]. But our work extends this paradigm by embedding the LLM reasoning within a closed-loop control framework, where symbolic decisions are continuously corrected by a learned neural controller, which is enabling fast convergence and robustness to noise.

2.3 Learning-Based Controllers and Delta Control

Learning-based controllers, especially deep neural networks, have demonstrated a strong performance in continuous control tasks due to their ability to approximate the nonlinear dynamics and also to generate smooth action trajectories [27]. For stabilization and fine-grained adjustments, delta controllers, which forecast incremental state changes rather than absolute actions, are particularly useful [28, 29].

Prior work has shown that delta-based control significantly improves convergence speed, reduces overshooting, and also enhances robustness in manipulation and navigation tasks [30]. These types of controllers are typically trained using supervised learning or reinforcement learning and also operate efficiently at inference time [31]. Neural network-based trajectory tracking for parallel robots has demonstrated that adaptive learning can also compensate for modeling uncertainties and external disturbances [32].

In our proposed technique, the neural delta controller has a crucial role in grounding symbolic decisions which are generated by the LLM. Rather than focusing on replacing the LLM, the controller complements it by making sure that each high-level decision is executed with minimal error. This strict integration especially enables our system to achieve both symbolic generalization and numerical precision. This combination is difficult to achieve with either component alone.

2.4 Spatial Reasoning and Relational Control Tasks

Spatial reasoning tasks involving relational concepts, including *left of*, *right of*, *above*, and *below*, have long been used as benchmarks for evaluating reasoning and control systems [33]. Classical approaches only rely on geometric constraints and optimization-based controllers, while learning-based methods often encode spatial relationships implicitly in the latent representations.

LLMs have shown favorable performance on symbolic spatial reasoning in purely textual domains, but also transferring this capability to physical or simulated control environments remains challenging [34]. The prior studies report that especially LLMs struggle with consistent spatial grounding, often producing actions that violate geometric constraints or converge slowly [35].

Our current work provides a systematic evaluation of spatial relational control using local LLMs, revealing consistent performance gaps in LLM-only settings. By incorporating a special neural execution module, we demonstrate that spatial reasoning can be reliably converted into precise control behavior, even when using relatively small local language models.

2.5 Local and Resource-Constrained Large Language Models

Most of the previous work on LLM-based robotics depends on large proprietary models accessed via cloud APIs [36]. While effective, such approaches raise concerns regarding reproducibility, latency, privacy, and deployment feasibility [37]. Recently, there has been growing interest in local LLMs that can run on consumer-grade hardware, driven by advances in model compression, quantization, and efficient architectures [38].

Local models such as Mistral [39], Phi [40], and LLaMA variants [41] provide a lower inference costs and also improved controllability but typically exhibit weaker reasoning performance compared to larger models [42]. These such models have been optimized for edge deployment scenarios, also including on-device translation, offline assistants, and autonomous robotics [43]. Few studies have also evaluated how this architectural integration with neural controllers can compensate for these limitations.

In our proposed work, we directly address this gap by conducting a comparative study across multiple local LLMs and demonstrating that the proposed neuro-symbolic architecture yields consistent gains regardless of model capacity. These findings suggest that architectural design is as significant as model scale in LLM-based control systems.

Previous research has explored LLMs for planning, neuro-symbolic reasoning, and learning-based control in isolation. However, current approaches either depend on open-loop reasoning, handcrafted symbolic planners, or also cloud-scale LLMs. Our work differs by the following points:

- Employing the local LLMs as symbolic planners,
- Embedding them within a closed-loop neuro-symbolic control architecture, and
- Demonstrating quantitative efficiency improvements in the spatial control tasks through tight integration with a neural delta controller.

These positions all show our current approach as a practical and scalable solution for grounded, interpretable, and also efficient LLM-based control.

3 Methodology

In addition to setting the problem and describing the design of each system component, this part provides the specific range of the suggested neuro-symbolic control that is our proposed framework. The methodology clearly differentiates between symbolic reasoning and continuous control while focusing on the modularity, interpretability, and efficiency.

3.1 Problem Setting and Notation

We consider a planar manipulation environment containing the following two entities:

- A *reference marker* (blue),
- A *target marker* (red).

The objective is to reposition the target marker such that it clearly satisfies a specified spatial relation regarding the reference marker, as described by a natural language instruction.

3.1.1 State Space

Let $\mathcal{W} \subset \mathbb{R}^2$ denote the bounded workspace. At discrete time step $t \in \{0, 1, \dots, T\}$, the environment state is represented as:

$$\mathbf{s}_t = (x_r^t, y_r^t, x_b^t, y_b^t)^\top \in \mathcal{S} \subseteq \mathbb{R}^4, \quad (1)$$

where (x_r^t, y_r^t) denote the Cartesian coordinates of the target marker and (x_b^t, y_b^t) denote those of the reference marker.

The workspace is bounded by:

$$\mathcal{W} = \{(x, y) \in \mathbb{R}^2 : 0 \leq x \leq C, 0 \leq y \leq C\}, \quad (2)$$

where $C \in \mathbb{R}^+$ is the maximum coordinate value. The state space is thus defined as the Cartesian product $\mathcal{S} = \mathcal{W} \times \mathcal{W}$.

3.1.2 Task Space

Each episode is associated with a task \mathcal{T} specified in natural language and mapped to one of four canonical spatial relations:

$$\mathcal{T} \in \Omega = \{\text{right_of}, \text{left_of}, \text{above}, \text{below}\}. \quad (3)$$

A margin parameter $m \in \mathbb{R}^+$ defines tolerance for task satisfaction. We formalize the task satisfaction conditions using the predicate $\mathcal{G} : \mathcal{S} \times \Omega \rightarrow \{0, 1\}$:

$$\mathcal{G}(\mathbf{s}_t, \mathcal{T}) = \begin{cases} \mathbb{1}[x_r^t \geq x_b^t + m] & \text{if } \mathcal{T} = \text{right_of}, \\ \mathbb{1}[x_r^t \leq x_b^t - m] & \text{if } \mathcal{T} = \text{left_of}, \\ \mathbb{1}[y_r^t \leq y_b^t - m] & \text{if } \mathcal{T} = \text{above}, \\ \mathbb{1}[y_r^t \geq y_b^t + m] & \text{if } \mathcal{T} = \text{below}, \end{cases} \quad (4)$$

where $\mathbb{1}[\cdot]$ denotes the indicator function returning 1 if the condition holds and 0 otherwise.

3.1.3 Action Space

The action space consists of incremental displacements bounded by maximum step size δ_{\max} :

$$\mathcal{A} = \{(\Delta x, \Delta y) \in \mathbb{R}^2 : |\Delta x| \leq \delta_{\max}, |\Delta y| \leq \delta_{\max}\}. \quad (5)$$

3.1.4 Objective

Given an initial state $\mathbf{s}_0 \sim \mathcal{P}_0$ and task $\mathcal{T} \sim \mathcal{P}_{\mathcal{T}}$, the goal is to compute a control policy $\pi : \mathcal{S} \times \Omega \rightarrow \mathcal{A}$ that:

1. Achieves task satisfaction within a finite horizon T :

$$\exists t^* \leq T : \mathcal{G}(\mathbf{s}_{t^*}, \mathcal{T}) = 1, \quad (6)$$

2. The expected number of control steps minimizes as follows:

$$\pi^* = \arg \min_{\pi} \mathbb{E}_{\mathbf{s}_0, \mathcal{T}} \left[\sum_{t=0}^{T-1} (1 - \mathcal{G}(\mathbf{s}_t, \mathcal{T})) \right], \quad (7)$$

3. Is robust to variations in language models and initial configurations.

3.2 Overall Neuro-Symbolic Architecture

The proposed framework decomposes decision-making into two interacting layers:

- **Symbolic reasoning layer** $\pi_{\text{sym}} : \mathcal{S} \times \Omega \rightarrow \mathcal{Z}$: responsible for task interpretation and semantic guidance.
- **Neural execution layer** $\pi_{\text{neu}} : \mathcal{S} \times \mathcal{Z} \rightarrow \mathcal{A}$: responsible for continuous control and motion refinement.

The composite policy is expressed as:

$$\pi(\mathbf{s}_t, \mathcal{T}) = \pi_{\text{neu}}(\mathbf{s}_t, \pi_{\text{sym}}(\mathbf{s}_t, \mathcal{T})), \quad (8)$$

where the symbolic latent space encoding task semantics denotes by \mathcal{Z} .

This separation follows the principle that symbolic abstractions and also the continuous dynamics should be managed by specialized modules rather than a monolithic policy.

3.3 Symbolic Reasoning with Local Large Language Models

The symbolic layer implements a locally deployed large language model (LLM) \mathcal{M}_{LLM} to process the natural language instruction and also reason about the desired spatial relationship.

3.3.1 LLM Input and Output Constraints

The LLM receives a structured prompt at each time step t as follows:

$$\mathbf{q}_t = \langle \mathcal{T}_{\text{nl}}, \psi(\mathbf{s}_t) \rangle, \quad (9)$$

where the natural language task description is denoted as \mathcal{T}_{nl} and $\psi : \mathcal{S} \rightarrow \Sigma^*$ is a serialization function mapping states to structured text over alphabet Σ .

To ensure the validity of the LLM that is constrained to output strictly formatted JSON responses as follows:

$$\mathbf{z}_t = \text{Parse}(\mathcal{M}_{\text{LLM}}(\mathbf{q}_t)) \in \mathcal{Z}, \quad (10)$$

where $\mathcal{Z} = \{0, 1, 2, 3\}$ corresponds to the four canonical spatial relations.

The LLM does not produce continuous actions directly. This constraint prevents instability, hallucinated coordinates, and non-physical behaviors commonly observed in LLM-only control.

3.3.2 Multi-Model LLM Integration

The framework supports interchangeable local LLMs:

$$\mathcal{M}_{\text{LLM}} \in \{\text{Mistral}, \text{Phi}, \text{LLaMA-3.2}\}, \quad (11)$$

without retraining the execution policy. This design enables systematic evaluation of language reasoning quality while keeping the control layer fixed.

3.4 Neural Delta Controller

The execution layer is implemented as a feedforward neural network $f_\theta : \mathbb{R}^d \rightarrow \mathbb{R}^2$ with parameters θ , trained to predict incremental displacements toward task satisfaction.

3.4.1 Input Encoding

The controller input at time t is constructed by concatenating normalized state features with the task encoding:

$$\mathbf{u}_t = \left[\frac{x_r^t}{C}, \frac{y_r^t}{C}, \frac{x_b^t}{C}, \frac{y_b^t}{C}, \phi(\mathcal{T}) \right]^\top \in \mathbb{R}^5, \quad (12)$$

where $\phi : \Omega \rightarrow [0, 1]$ is a scalar encoding of the task relation defined as:

$$\phi(\mathcal{T}) = \frac{\text{idx}(\mathcal{T})}{|\Omega| - 1}, \quad (13)$$

with $\text{idx}(\cdot)$ returning the index of the task in Ω .

Alternatively, a one-hot encoding $\phi_{\text{oh}} : \Omega \rightarrow \{0, 1\}^{|\Omega|}$ may be used:

$$\phi_{\text{oh}}(\mathcal{T}) = \mathbf{e}_{\text{idx}(\mathcal{T})} \in \{0, 1\}^4, \quad (14)$$

where \mathbf{e}_i denotes the i -th standard basis vector, yielding input dimension $d = 8$.

3.4.2 Network Architecture

The neural controller consists of L fully-connected layers:

$$f_\theta(\mathbf{u}) = \mathbf{W}_L \sigma(\mathbf{W}_{L-1} \sigma(\cdots \sigma(\mathbf{W}_1 \mathbf{u} + \mathbf{b}_1) \cdots) + \mathbf{b}_{L-1}) + \mathbf{b}_L, \quad (15)$$

where $\sigma(\cdot) = \max(0, \cdot)$ is the ReLU activation, $\mathbf{W}_l \in \mathbb{R}^{n_l \times n_{l-1}}$ are weight matrices, and $\mathbf{b}_l \in \mathbb{R}^{n_l}$ are bias vectors.

The output layer applies hyperbolic tangent activation to bound displacements:

$$(\Delta x_t, \Delta y_t) = \delta_{\max} \cdot \tanh(f_\theta(\mathbf{u}_t)) \in [-\delta_{\max}, \delta_{\max}]^2. \quad (16)$$

3.4.3 Output and State Transition

The predicted displacement updates the target marker position via the transition function $\mathcal{F} : \mathcal{S} \times \mathcal{A} \rightarrow \mathcal{S}$:

$$x_r^{t+1} = \text{clip}(x_r^t + \Delta x_t, 0, C), \quad (17)$$

$$y_r^{t+1} = \text{clip}(y_r^t + \Delta y_t, 0, C), \quad (18)$$

where the clipping function enforces workspace boundaries:

$$\text{clip}(z, a, b) = \min(\max(z, a), b). \quad (19)$$

Delta-based control reduces overshooting and improves stability compared to absolute coordinate prediction. As shown in Fig. 2, the proposed framework decouples symbolic reasoning from continuous control by delegating language understanding to a local LLM and motion execution to a neural delta controller.

3.5 Training Procedure

The neural controller is trained using supervised learning on synthetically generated trajectories.

3.5.1 Dataset Generation

Each training sample consists of a state-task-displacement tuple:

$$\mathcal{D} = \left\{ \left(\mathbf{s}^{(i)}, \mathcal{T}^{(i)}, \Delta \mathbf{p}^{*(i)} \right) \right\}_{i=1}^N, \quad (20)$$

where $\mathbf{s}^{(i)} \sim \text{Uniform}(\mathcal{S})$, $\mathcal{T}^{(i)} \sim \text{Uniform}(\Omega)$, and $\Delta \mathbf{p}^{*(i)} = (\Delta x^*, \Delta y^*)$ is the target displacement that moves the target marker closer to task satisfaction.

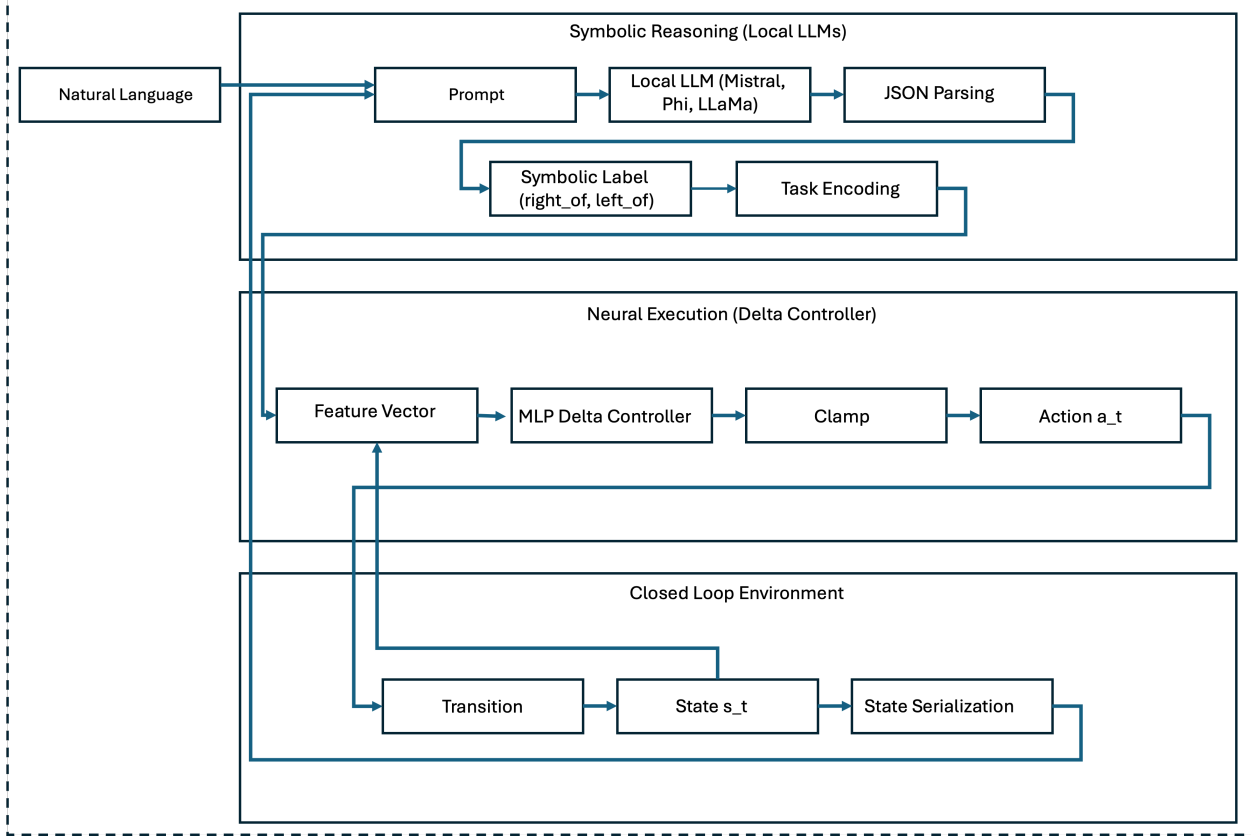


Figure 2: Overview of the proposed neuro-symbolic control framework. A local large language model performs symbolic reasoning over language instructions and environment state, producing a discrete task label. This symbolic output conditions a neural delta controller that executes bounded continuous actions in a closed-loop environment, enabling stable, efficient, and interpretable control.

3.5.2 Target Displacement Computation

The optimal displacement is computed as the direction toward the goal region scaled by step size $\alpha \in (0, 1]$. For $\mathcal{T} = \text{right_of}$:

$$\Delta x^* = \alpha \cdot \max(0, (x_b + m) - x_r), \quad \Delta y^* = 0. \quad (21)$$

Analogous expressions hold for other spatial relations:

$$\text{left_of} : \quad \Delta x^* = -\alpha \cdot \max(0, x_r - (x_b - m)), \quad \Delta y^* = 0, \quad (22)$$

$$\text{above} : \quad \Delta x^* = 0, \quad \Delta y^* = -\alpha \cdot \max(0, y_r - (y_b - m)), \quad (23)$$

$$\text{below} : \quad \Delta x^* = 0, \quad \Delta y^* = \alpha \cdot \max(0, (y_b + m) - y_r). \quad (24)$$

3.5.3 Loss Function

The mean squared error between the target and forecast displacements is the definition of the loss function:

$$\mathcal{L}(\theta) = \frac{1}{N} \sum_{i=1}^N \left\| f_\theta(\mathbf{u}^{(i)}) - \Delta \mathbf{p}^{*(i)} \right\|_2^2. \quad (25)$$

To encourage smooth trajectories, an optional regularization term penalizes large displacement magnitudes:

$$\mathcal{L}_{\text{reg}}(\theta) = \mathcal{L}(\theta) + \lambda \cdot \frac{1}{N} \sum_{i=1}^N \left\| f_\theta(\mathbf{u}^{(i)}) \right\|_2^2, \quad (26)$$

where $\lambda \geq 0$ is the regularization coefficient.

Algorithm 1: Neuro-Symbolic Closed-Loop Control

Input: Initial state \mathbf{s}_0 , task \mathcal{T} , horizon T , LLM \mathcal{M}_{LLM} , controller f_θ

Output: Final state \mathbf{s}_{t^*} , success flag, step count

$t \leftarrow 0$;

while $t < T$ and $\mathcal{G}(\mathbf{s}_t, \mathcal{T}) = 0$ **do**

Construct prompt $\mathbf{q}_t \leftarrow \langle \mathcal{T}_{\text{nl}}, \psi(\mathbf{s}_t) \rangle$;
 Symbolic reasoning $\mathbf{z}_t \leftarrow \text{Parse}(\mathcal{M}_{\text{LLM}}(\mathbf{q}_t))$;
 Encode input $\mathbf{u}_t \leftarrow [\mathbf{s}_t / C, \phi(\mathbf{z}_t)]^\top$;
 Compute action $(\Delta x_t, \Delta y_t) \leftarrow f_\theta(\mathbf{u}_t)$;
 Update state $\mathbf{s}_{t+1} \leftarrow \mathcal{F}(\mathbf{s}_t, (\Delta x_t, \Delta y_t))$;
 $t \leftarrow t + 1$;

return $\mathbf{s}_t, \mathcal{G}(\mathbf{s}_t, \mathcal{T}), t$;

3.5.4 Optimization

Parameters θ are optimized using stochastic gradient descent with the Adam optimizer:

$$\theta_{k+1} = \theta_k - \eta \cdot \frac{\hat{\mathbf{m}}_k}{\sqrt{\hat{\mathbf{v}}_k} + \epsilon}, \quad (27)$$

where the learning rate is denoted by η , $\hat{\mathbf{m}}_k$, $\hat{\mathbf{v}}_k$ are bias-corrected moment estimates, and a small constant for numerical stability is denoted by ϵ .

This formulation advocates a smooth, task-directed motion and more generalization across tasks.

3.6 Closed-Loop Control Strategy

The following process governs the closed-loop operation of the system as follows:

This feedback loop enables online correction and robust convergence even under imperfect symbolic reasoning.

3.7 Distance-to-Goal Metric

To analyze convergence behavior, we define a distance-to-goal metric $d : \mathcal{S} \times \Omega \rightarrow \mathbb{R}_{\geq 0}$:

$$d(\mathbf{s}_t, \mathcal{T}) = \begin{cases} \max(0, (x_b^t + m) - x_r^t) & \text{if } \mathcal{T} = \text{right_of}, \\ \max(0, x_r^t - (x_b^t - m)) & \text{if } \mathcal{T} = \text{left_of}, \\ \max(0, y_r^t - (y_b^t - m)) & \text{if } \mathcal{T} = \text{above}, \\ \max(0, (y_b^t + m) - y_r^t) & \text{if } \mathcal{T} = \text{below}. \end{cases} \quad (28)$$

The following characteristics are satisfied by this metric:

1. **Non-negativity:** $d(\mathbf{s}_t, \mathcal{T}) \geq 0$ for all $\mathbf{s}_t \in \mathcal{S}, \mathcal{T} \in \Omega$.
2. **Goal identification:** $d(\mathbf{s}_t, \mathcal{T}) = 0 \Leftrightarrow \mathcal{G}(\mathbf{s}_t, \mathcal{T}) = 1$.
3. **Continuity:** d is continuous in \mathbf{s}_t .

For cross-episode comparison, we define the normalized distance:

$$\bar{d}_t = \frac{d(\mathbf{s}_t, \mathcal{T})}{d(\mathbf{s}_0, \mathcal{T}) + \epsilon}, \quad (29)$$

where $\epsilon > 0$ ensures numerical stability when $d(\mathbf{s}_0, \mathcal{T}) \approx 0$.

3.8 Baselines and Ablation Configurations

We evaluate three separate system variants to isolate component contributions:

3.8.1 LLM-Only Control

The LLM directly predicts absolute target coordinates:

$$(\hat{x}_r, \hat{y}_r) = \mathcal{M}_{\text{LLM}}(\mathbf{q}_t), \quad (30)$$

also with the displacement computed as follows:

$$(\Delta x_t, \Delta y_t) = (\hat{x}_r - x_r^t, \hat{y}_r - y_r^t). \quad (31)$$

This kind of arrangement is prone to slower convergence, large variation, and hallucinated coordinates.

3.8.2 DL-Only Control

Without using LLM reasoning, the neural controller uses a set, predetermined job encoding:

$$(\Delta x_t, \Delta y_t) = f_{\theta}(\mathbf{u}_t), \quad \text{where } \phi(\mathcal{T}) = \text{const.} \quad (32)$$

The neural controller's ability to maintain control in the absence of symbolic guidance is isolated by this ablation.

3.8.3 LLM+DL (Proposed)

The full neuro-symbolic integration:

$$(\Delta x_t, \Delta y_t) = f_{\theta}(\mathbf{s}_t, \pi_{\text{sym}}(\mathbf{s}_t, \mathcal{T})), \quad (33)$$

That is combining symbolic task interpretation with neural execution. The proposal technique delivers better robustness across language models, faster convergence, and higher success rates by clearly separating thinking from execution. In addition, this design makes it possible to systematically analyze the quality of LLM reasoning without confusing it with low-level control performance.

4 Experimental Setup and Results

This section clearly demonstrated the details of the experimental evaluation of the proposed neuro-symbolic control framework. We establish the baseline processes, evaluation metrics, experimental design, and quantitative results. We designed the experiments in such a way that they ensure reproducibility, controlled ablation, and statistically significant comparisons between control strategies and language models.

4.1 Experimental Setup

4.1.1 Environment Configuration

Every experiment is carried out in a planar simulated environment with two identifiable markers: a target marker (red) and a reference marker (blue). The workspace is defined as a bounded square region as follows; $\mathcal{W} = [0, C]^2 \subset \mathbb{R}^2$ with $C = 800$ pixels.

At the beginning of each episode, both markers are initialized via independent uniform sampling:

$$\mathbf{p}_r^0, \mathbf{p}_b^0 \sim \text{Uniform}(\mathcal{W}). \quad (34)$$

The control objective is to reposition the target marker such that it satisfies a specified spatial relation with respect to the reference marker within a fixed time horizon T .

4.1.2 Task Specification

We evaluate four canonical spatial relations constituting the task space Ω :

$$\Omega = \{\text{right_of}, \text{left_of}, \text{above}, \text{below}\}. \quad (35)$$

A task $\mathcal{T} \in \Omega$ is considered successfully completed if the corresponding geometric constraint is satisfied with margin $m = 50$ pixels:

$$\mathcal{G}(\mathbf{s}_t, \mathcal{T}) = 1, \quad \text{for some } t \leq T. \quad (36)$$

Each task is presented to the system via natural language instruction, requiring interpretation by the symbolic reasoning module.

4.1.3 Compared Methods

To isolate the contributions of symbolic reasoning and neural execution, we evaluate three control paradigms:

LLM-Only Control. In this baseline, a large language model directly predicts absolute target coordinates (\hat{x}_r, \hat{y}_r) at each time step based on the current state \mathbf{s}_t and natural language instruction \mathcal{T}_{nl} . The displacement is computed as:

$$(\Delta x_t, \Delta y_t) = (\hat{x}_r - x_r^t, \hat{y}_r - y_r^t). \quad (37)$$

No learned motion prior is applied. This baseline evaluates the capacity of LLMs to perform spatial reasoning and continuous control without neural assistance.

DL-Only Control. This baseline employs the neural delta controller exclusively with a fixed, ground-truth task encoding:

$$(\Delta x_t, \Delta y_t) = f_\theta(\mathbf{u}_t), \quad \phi(\mathcal{T}) = \phi^*, \quad (38)$$

where ϕ^* denotes the oracle task encoding. No LLM reasoning is invoked during execution. This configuration evaluates the controller's performance when task semantics are perfectly specified, establishing an upper bound on neural execution quality.

LLM+DL (Proposed). The proposed neuro-symbolic method combines symbolic reasoning with neural execution:

$$(\Delta x_t, \Delta y_t) = f_\theta(\mathbf{u}_t, \pi_{\text{sym}}(\mathbf{s}_t, \mathcal{T})). \quad (39)$$

A local LLM interprets the natural language instruction and outputs a symbolic relation label $\mathbf{z}_t \in \mathcal{Z}$, which conditions the neural delta controller. The controller predicts incremental displacements in a closed-loop manner, enabling stable and efficient convergence.

4.1.4 Language Models

All symbolic reasoning is performed using locally deployed large language models to ensure reproducibility, low-latency inference, and independence from external APIs. We evaluate the following models:

- **Mistral-7B:** A 7-billion parameter model optimized for instruction following and efficient inference.
- **Phi-2:** A compact 2.7-billion parameter model designed for resource-constrained deployment.
- **LLaMA-3.2:** Meta's open-weight model with strong reasoning capabilities.

The neural controller f_θ remains fixed across all experiments, enabling controlled comparison of symbolic reasoning quality across models while isolating the contribution of the neural execution layer.

4.1.5 Evaluation Protocol

For each combination of this proposed method, language model, and task, we conduct $N = 20$ independent episodes with randomized initial configurations. We show mean performance with standard deviation to quantify variability. In Fig. 3, we can see that the proposed LLM+DL framework consistently achieves higher success rates across all spatial tasks when compared to both LLM-only and DL-only baselines.

4.1.6 Evaluation Metrics

We assess performance using the following metrics:

Success Rate (SR) The fraction of episodes achieving task satisfaction within the time horizon:

$$\text{SR} = \frac{1}{N} \sum_{i=1}^N \mathbb{1} \left[\exists t \leq T : \mathcal{G}(\mathbf{s}_t^{(i)}, \mathcal{T}) = 1 \right]. \quad (40)$$

Average Steps (AS) The mean number of control steps required for successful episodes:

$$\text{AS} = \frac{1}{|\mathcal{S}_{\text{succ}}|} \sum_{i \in \mathcal{S}_{\text{succ}}} t_i^*, \quad (41)$$

where $\mathcal{S}_{\text{succ}}$ denotes the set of successful episodes and t_i^* is the termination step.

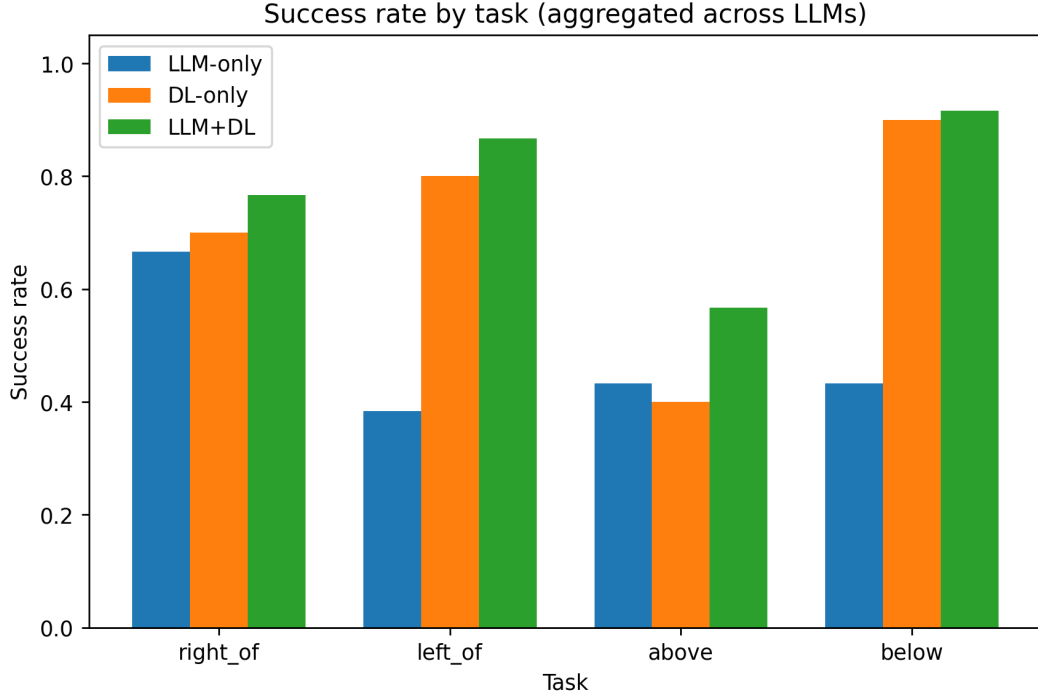


Figure 3: Success rate aggregated across all language models for each spatial task. The proposed LLM+DL framework consistently outperforms LLM-only and DL-only baselines, demonstrating the effectiveness of neuro-symbolic integration.

Normalized Distance-to-Goal The task-specific geometric distance to the satisfaction boundary, normalized by initial distance:

$$\bar{d}_t = \frac{d(\mathbf{s}_t, \mathcal{T})}{d(\mathbf{s}_0, \mathcal{T}) + \epsilon}. \quad (42)$$

Relative Improvement Metrics To quantify the benefit of neuro-symbolic integration, we compute:

- **Success Rate Improvement:** $\Delta SR = SR_{LLM+DL} - SR_{LLM-only}$
- **Step Reduction:** $\rho = \frac{AS_{LLM-only} - AS_{LLM+DL}}{AS_{LLM-only}} \times 100\%$
- **Speedup Factor:** $\sigma = \frac{AS_{LLM-only}}{AS_{LLM+DL}}$

4.2 Results

4.2.1 Overall Performance Comparison

The average number of steps and success rate for each technique, task, and language model for the `right_of` task are summarized in Table 1. The supplemental material contains the full results for each task.

Several observations emerge from the results:

- For the consistent improvement, across all language models, the suggested LLM+DL framework produces success rates that are either greater or equivalent to those of LLM-only control, with significant drops in average steps.
- For the efficiency gains, depending on the underlying language model, the neural delta controller allows convergence in many fewer steps, with speedups ranging from $2.52 \times$ to $5.82 \times$.
- For the compensation for weak reasoning, the Phi model shows the best LLM+DL success rate (0.85) but the lowest LLM-only success rate (0.60), indicating that the neural controller successfully makes up for weaker symbolic reasoning.

Table 1: Performance comparison across control methods and LLMs.

LLM Model	Method	Task	Success Rate	Avg. Steps
-	DL-only	right_of	0.70	1.35
Mistral	LLM-only	right_of	0.70	3.60
Mistral	LLM+DL	right_of	0.70	1.15
Phi	LLM-only	right_of	0.60	4.95
Phi	LLM+DL	right_of	0.85	0.85
LLaMA-3.2	LLM-only	right_of	0.70	3.40
LLaMA-3.2	LLM+DL	right_of	0.75	1.35

4.2.2 Convergence Analysis

According to Fig. 4, LLM+DL typically reduces the number of necessary control steps by more than 70%.

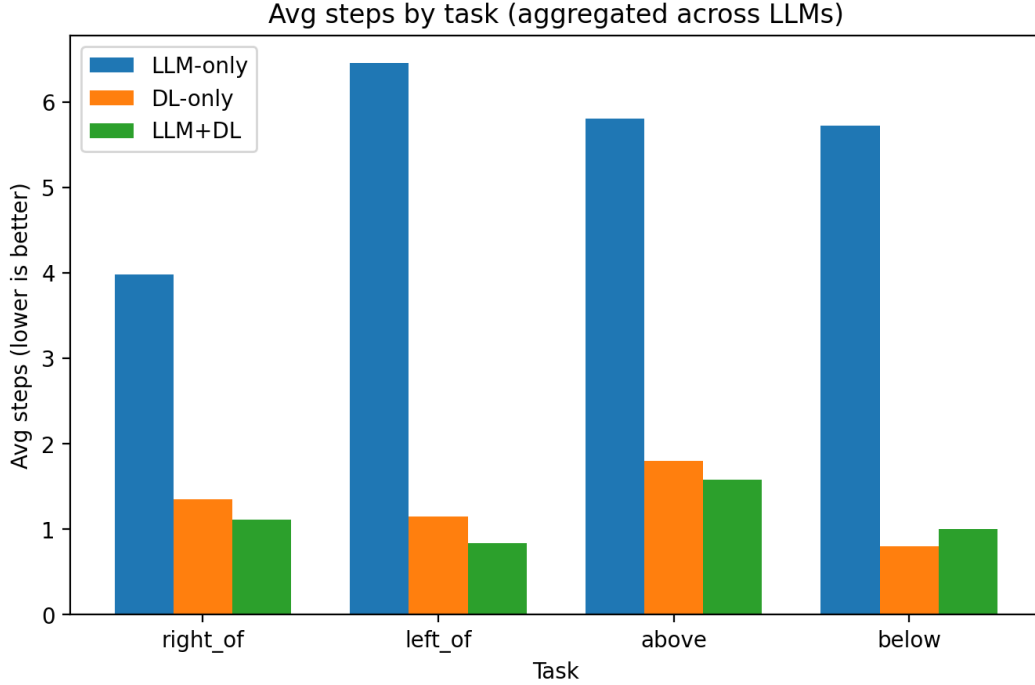


Figure 4: Total average number of control steps for all language models. Compared to LLM-only control, the LLM+DL framework converges far more quickly, resulting in a step reduction of more than 70% for all jobs.

Each method's unique qualities are shown by the convergence behavior:

- For the LLM-only, it shows oscillatory behavior as a result of inaccurate coordinate predictions and sluggish convergence with large variance. The distance-to-goal curve exhibits numerous reversals and non-monotonic descent.
- For the DL-only, when given Oracle task encoding, it converges quickly and monotonically. Nevertheless, new task descriptions or variations in natural language cannot be accommodated by this setup.
- For the LLM+DL, it retains the capacity to understand normal language instructions while achieving quick, consistent convergence on par with DL-only. While symbolic reasoning offers high-level semantic guidance, the neural delta controller guarantees smooth paths.

The normalized distance-to-goal over time is shown in Fig. 5, which highlights the LLM+DL framework's faster and more stable convergence.

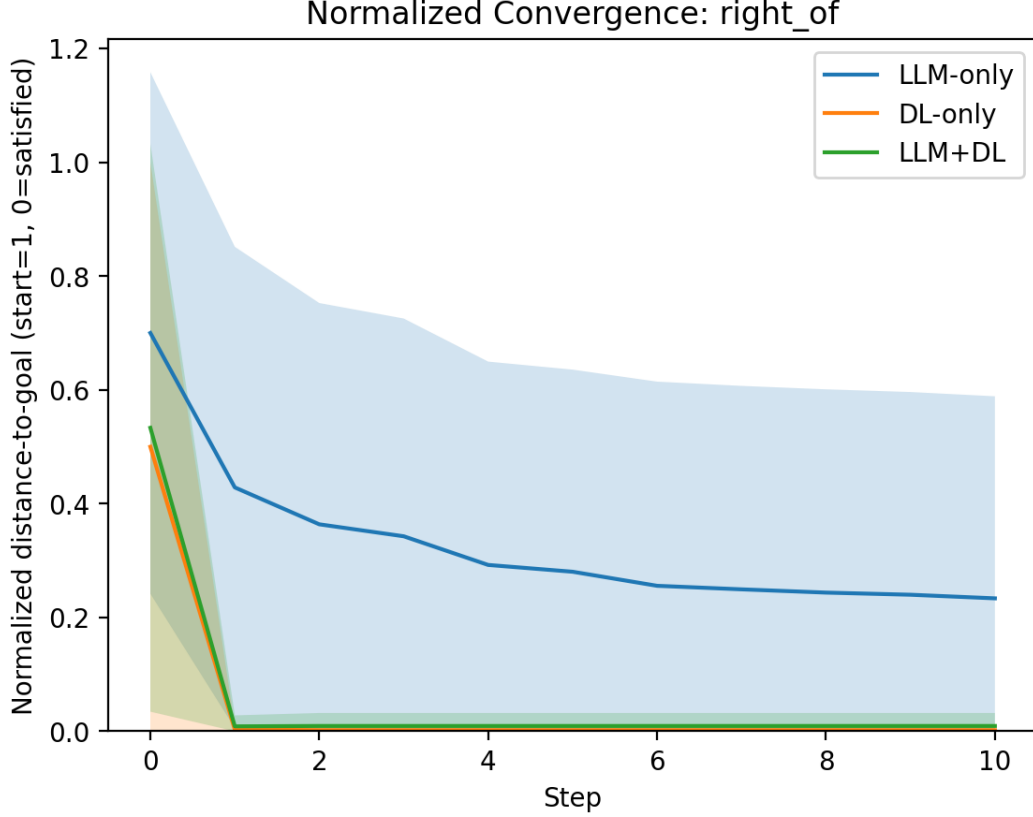


Figure 5: Normalized distance-to-goal over time for the `right_of` task. LLM+DL exhibits fast, monotonic convergence with low variance, whereas LLM-only control shows slower and less stable behavior.

Table 2: Relative improvement of LLM+DL over LLM-only (mean \pm std).

Task	Δ Success	Step Reduction (%)	Speedup (\times)
right_of	0.10 ± 0.13	70.4 ± 11.4	3.82 ± 1.76
left_of	0.48 ± 0.23	85.9 ± 7.7	8.83 ± 4.93
above	0.13 ± 0.25	72.4 ± 9.2	3.87 ± 1.09
below	0.48 ± 0.10	82.4 ± 3.3	5.81 ± 1.07

4.2.3 Relative Improvement Analysis

To quantify the benefit of neuro-symbolic integration across all tasks, Table 2 reports aggregated statistics comparing LLM+DL to LLM-only control. Results are averaged across all three language models.

Key findings include:

- For the significant speedup, for all tasks, the suggested method delivers an average speedup of $5.58\times$, with a maximum speedup of $8.83\times$ for the `left_of` relation.
- For the task-dependent gains, compared to orthogonal relations (`right_of`, `above`), lateral relations (`left_of`, `below`) show greater increases in speedup and success rate (Δ SR = 0.48). This imbalance implies that some spatial interactions are more difficult for LLM-only management because of incorrect or hallucinated coordinate predictions.
- Regardless of the kind of work, step reduction consistently surpasses 70%, indicating that the neural delta controller significantly increases control efficiency.

As summarized in Fig. 6, the proposed method achieves speedups of up to $8.83\times$ over LLM-only control.

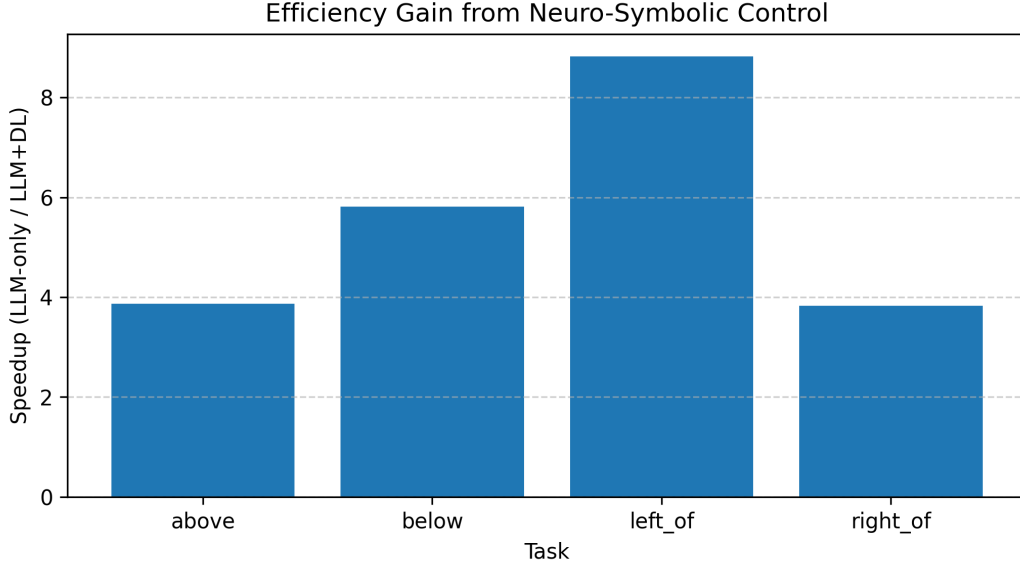


Figure 6: Speedup of LLM+DL relative to LLM-only control aggregated across language models. The proposed framework achieves substantial efficiency gains, with speedups of up to $8.83\times$ depending on the spatial relation.

4.2.4 Robustness Across Language Models

Performance gains are consistent across all evaluated language models, with several notable observations:

- For the model-agnostic improvement, the LLM+DL framework enhances all three models performance, suggesting that architectural decomposition, rather than language model capacity or scale, is the source of the advantages.
- For the compensation effect, even in situations where LLM-only control operates badly, robust performance is made possible by the neural controller’s compensation for inferior symbolic thinking. This is especially true for Phi, where LLM+DL outperforms the model even with fewer parameters.
- To the decreased variance, the LLM+DL performs more consistently across episodes and beginning settings, as seen by a significantly lower standard deviation of success rates than LLM-only.

The performance improvements of the neuro-symbolic framework hold true for all assessed local LLMs, as shown in Fig. 7.

4.2.5 Ablation: Component Contribution

We calculate the performance difference between approaches in order to further isolate each component’s contribution:

$$\Delta_{\text{symbolic}} = \text{SR}_{\text{LLM+DL}} - \text{SR}_{\text{DL-only}}, \quad (43)$$

$$\Delta_{\text{neural}} = \text{SR}_{\text{LLM+DL}} - \text{SR}_{\text{LLM-only}}. \quad (44)$$

Averaged across all configurations, we observe $\Delta_{\text{symbolic}} = 0.12$ and $\Delta_{\text{neural}} = 0.30$, indicating that both components contribute meaningfully to overall performance, with the neural controller providing the larger marginal improvement. We can infer the following inferences from the experimental results:

- Control using LLM alone is ineffective: Particularly for spatial manipulation tasks requiring numerical precision, direct coordinate prediction by LLMs results in sluggish convergence, significant variance, and inconsistent behavior.
- DL-only control lacks semantic flexibility: While the neural controller converges rapidly with oracle task encoding, it cannot interpret natural language instructions or generalize to novel task formulations.

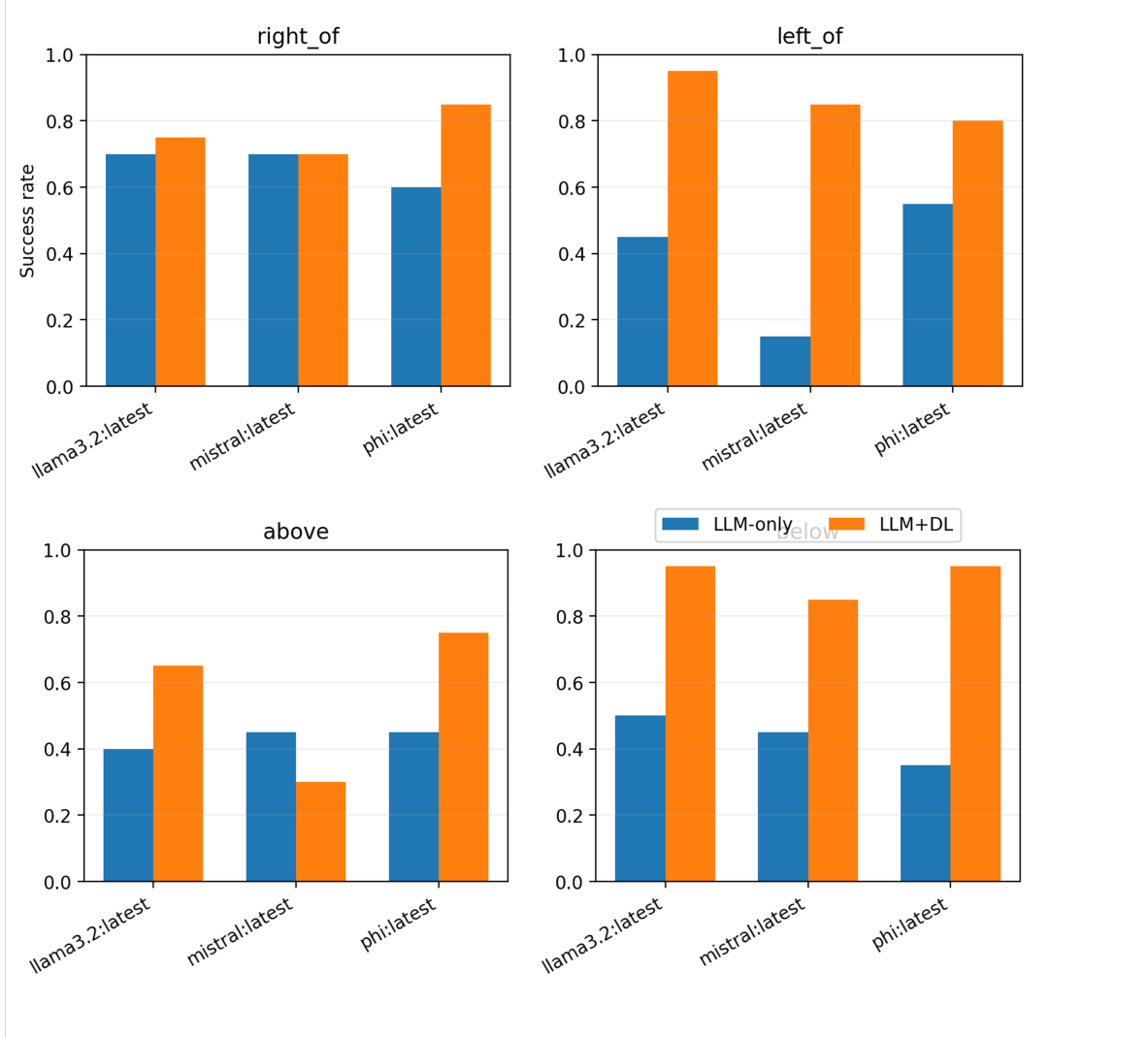


Figure 7: Success rate by language model and task. The suggested LLM+DL framework consistently improves performance on Mistral, Phi, and LLaMA-3.2, demonstrating resilience to scale and language model selection.

- Neuro-symbolic integration works well: By combining the complementing advantages of neural control and symbolic thinking, the suggested LLM+DL paradigm achieves the following:
 - Up to $8.83 \times$ speedup over LLM-only control
 - Average success rate improvement of 0.30
 - Consistent gains across all language models and tasks
 - Reduced variance and improved robustness
- Architectural design matters: The neuro-symbolic decomposition offers advantages independent of underlying model capability, as evidenced by the performance gains that are consistent across language models of different scales.

These results support the main hypothesis that more effective, reliable, and comprehensible behavior is produced in language-conditioned manipulation tasks when symbolic thinking and continuous control are separated.

5 Discussion and Conclusion

The experimental findings show that the efficiency, stability, and resilience of language-conditioned control significantly increase when symbolic reasoning and continuous control are explicitly separated. The suggested neuro-symbolic architecture avoids the instability, sluggish convergence, and hallucinated actions frequently seen in monolithic LLM-based control systems by assigning high-level semantic interpretation to a big language model and low-level execution to a neural delta controller.

The suggested LLM+DL method continuously beats LLM-only baselines in both success rate and convergence speed across all assessed spatial tasks and local language models. While preserving or increasing task success rates, average step reductions surpass 70%, with speedups up to $8.83\times$ in some setups. Interestingly, these improvements hold true even with poorer or smaller language models, suggesting that the neural execution layer successfully makes up for flawed symbolic thinking.

In order to stabilize execution, the neural delta controller is essential. It demonstrates the efficacy of learning task-agnostic motion primitives by generalizing across tasks and language models without retraining after being trained exclusively on synthetic geometric data. Unlike opaque end-to-end LLM control, restricting the LLM to symbolic outputs allows failures to be clearly attributed to either semantic reasoning or execution, which further improves interpretability and debuggability.

Practically speaking, the framework provides a number of deployment benefits. Real-time execution is made possible by the lightweight neural controller, independent component updates are made possible by the modular architecture, and local LLM inference minimizes external dependencies. Because of these characteristics, the method works effectively in environments where resources are limited and safety is crucial.

The present analysis is restricted to planar environments with perfect state observability and primitive spatial linkages, despite these advantages. The expressiveness of compositional or temporally extended instructions is limited by the symbolic layer's operation over a fixed task set. Furthermore, even if local LLMs lower reliance and cost, stochastic outputs and inference latency are still factors to take into account.

This framework will be expanded in the future to include real-world robotic platforms, richer symbolic representations, hierarchical and compositional task structures, and multi-object and vision-based environments. One interesting way to scale the technique is to incorporate long-horizon planning and perception-driven state estimation.

To sum up, our research gives compelling empirical proof that neuro-symbolic integration provides a rational and practical means of fusing language comprehension with ongoing control. The suggested framework promotes the creation of dependable, comprehensible, and effective language-guided embodied systems by utilizing the complementing capabilities of big language models and neural controllers.

References

- [1] D. Bandyopadhyay, S. Bhattacharjee, and A. Ekbal, “Thinking machines: A survey of LLM based reasoning strategies,” *arXiv preprint arXiv:2503.10814*, 2025.
- [2] Y. Zhang, H. Wang, S. Feng, Z. Tan, X. Han, T. He, and Y. Tsvetkov, “Can LLM graph reasoning generalize beyond pattern memorization?,” *arXiv preprint arXiv:2406.15992*, 2024.
- [3] L. Liu, A. Nair, T. Peng, S. Desai, M. Gupta, K. Mehta, and P. Singh, “Optimizing task planning efficiency in LLMs: Beyond closed-loop systems,” *Authorea Preprints*, 2024.
- [4] S. Banerjee, A. Agarwal, and S. Singla, “LLMs will always hallucinate, and we need to live with this,” in *Proc. Intelligent Systems Conference*, Cham, Switzerland: Springer, Aug. 2025, pp. 624–648.
- [5] L. Huang, W. Yu, W. Ma, W. Zhong, Z. Feng, H. Wang, and T. Liu, “A survey on hallucination in large language models: Principles, taxonomy, challenges, and open questions,” *ACM Transactions on Information Systems*, vol. 43, no. 2, pp. 1–55, 2025.
- [6] C. Tang, B. Abbatematteo, J. Hu, R. Chandra, R. Martín-Martín, and P. Stone, “Deep reinforcement learning for robotics: A survey of real-world successes,” *Annual Review of Control, Robotics, and Autonomous Systems*, vol. 8, pp. 153–178, 2025.
- [7] Q. Du, B. Li, Y. Du, S. Su, T. Fu, Z. Zhan, and C. Wang, “Fast task planning with neuro-symbolic relaxation,” *arXiv preprint arXiv:2507.15975*, 2025.
- [8] S. Bhat, et al., “Grounding large language models for robot task planning using closed-loop state feedback,” *arXiv preprint arXiv:2402.08546*, 2024.

- [9] W. Su, “Do large language models (really) need statistical foundations?,” *arXiv preprint arXiv:2505.19145*, 2025.
- [10] V. Ennasmo, C. Featherstonehaugh, X. Konstantinopoulos, and Z. Huntington, “Structural embedding projection for contextual large language model inference,” *arXiv preprint arXiv:2501.18826*, 2025.
- [11] Y. Kim, J. Choi, and S. Lee, “A survey on integration of large language models with intelligent robots,” *Intelligent Service Robotics*, 2024.
- [12] A. Zeng, et al., “Large language models for robotics: A survey,” *arXiv preprint arXiv:2311.07226*, 2023.
- [13] W. Huang, P. Abbeel, D. Pathak, and I. Mordatch, “Language models as zero-shot planners: Extracting actionable knowledge for embodied agents,” in *Proc. ICML*, 2022.
- [14] M. Ahn, et al., “Do as I can, not as I say: Grounding language in robotic affordances,” in *Proc. CoRL*, 2022.
- [15] D. Driess, et al., “PaLM-E: An embodied multimodal language model,” in *Proc. ICML*, 2023.
- [16] J. Liang, et al., “Code as policies: Language model programs for embodied control,” in *Proc. ICRA*, 2023.
- [17] Y. Liu, et al., “Large language models for robotics: Opportunities, challenges, and perspectives,” *Science China Information Sciences*, 2024.
- [18] J. Wang, et al., “A survey of robot intelligence with large language models,” *Applied Sciences*, vol. 14, no. 19, 2024.
- [19] Y. Chen, J. Arkin, Y. Zhang, et al., “AutoTAMP: Autoregressive task and motion planning with LLMs as translators and checkers,” in *Proc. ICRA*, 2024.
- [20] A. Garcez and L. Lamb, “Neurosymbolic AI: The 3rd wave,” *Artificial Intelligence Review*, vol. 56, pp. 12387–12406, 2023.
- [21] Z. Wan, et al., “Towards cognitive AI systems: A survey and prospective on neuro-symbolic AI,” *arXiv preprint arXiv:2401.01040*, 2024.
- [22] L. De Raedt, S. Dumancic, R. Manhaeve, and G. Marra, “From statistical relational to neurosymbolic artificial intelligence: A survey,” *Artificial Intelligence*, vol. 328, 2024.
- [23] B. C. Colelough, et al., “Neuro-symbolic AI in 2024: A systematic review,” in *CEUR Workshop Proceedings*, 2024.
- [24] C. R. Garrett, R. Chitnis, R. M. Holladay, et al., “Integrated task and motion planning,” *Annual Review of Control, Robotics, and Autonomous Systems*, vol. 4, pp. 265–293, 2021.
- [25] Z. Zhao, et al., “A survey of task planning with large language models,” *Intelligent Computing*, 2024.
- [26] B. Bousetouane, “Agentic LLM-based robotic systems for real-world applications: A review,” *Frontiers in Robotics and AI*, 2025.
- [27] K. Arulkumaran, M. P. Deisenroth, M. Brundage, and A. A. Bharath, “Deep reinforcement learning: A brief survey,” *IEEE Signal Processing Magazine*, vol. 34, no. 6, pp. 26–38, 2017.
- [28] L. M. Thanh, L. H. Thuong, P. T. Loc, and C.-N. Nguyen, “Delta robot control using single neuron PID algorithms based on recurrent fuzzy neural network identifiers,” *Int. J. Mech. Eng. Robot. Res.*, vol. 9, no. 10, pp. 1411–1418, 2020.
- [29] M. Nguyen, et al., “Inverse kinematic control of a delta robot using neural networks in real-time,” *Robotics*, vol. 10, no. 4, 2021.
- [30] Y. Zhang, et al., “Fixed-time incremental neural control for manipulator based on composite learning with input saturation,” *Actuators*, vol. 11, no. 12, 2022.
- [31] M. dos S. Lima, et al., “Delta robot control by learning systems: Harnessing the power of deep reinforcement learning algorithms,” *J. Control, Automation and Electrical Systems*, 2024.
- [32] S. Khosravi and A. Akbari, “Experimental study on a novel simultaneous control and identification of a 3-DOF delta robot using model reference adaptive control,” *Mechatronics*, vol. 86, 2022.
- [33] B. Chen, Z. Xu, S. Kirmani, et al., “SpatialVLM: Endowing vision-language models with spatial reasoning capabilities,” in *Proc. CVPR*, 2024.
- [34] K. Rana, J. Haviland, S. Garg, et al., “SayPlan: Grounding large language models using 3D scene graphs for scalable robot task planning,” in *Proc. CoRL*, 2023.
- [35] W. Hunt, S. D. Ramchurn, and M. D. Soorati, “A survey of language-based communication in robotics,” *arXiv preprint arXiv:2406.04086*, 2024.

- [36] J. Wang, et al., “Large language models for robotics: Opportunities, challenges, and perspectives,” *arXiv preprint*, 2024.
- [37] B. Amin, “Mistral expands its reach in the SLM space with Minstral models,” *TechTalks*, October 2024.
- [38] Z. Wan, et al., “A review on edge large language models: Design, execution, and applications,” *arXiv preprint arXiv:2410.11845*, 2024.
- [39] A. Q. Jiang, et al., “Mistral 7B,” *arXiv preprint arXiv:2310.06825*, 2023.
- [40] M. Abdin, et al., “Phi-3 technical report: A highly capable language model locally on your phone,” *arXiv preprint arXiv:2404.14219*, 2024.
- [41] H. Touvron, et al., “LLaMA: Open and efficient foundation language models,” *arXiv preprint arXiv:2302.13971*, 2023.
- [42] Data Science Dojo, “Phi 3 and beyond: Top small language models of 2024,” 2024.
- [43] Mistral AI, “Introducing Les Ministraux: Edge-optimized models,” October 2024.

Supplementary Material

Additional experimental data and analysis that corroborate the conclusions in the main paper are provided in this supplementary section. These findings provide more clear and precise information about ablation results, task-wise convergence patterns, and model-specific behavior. Every experiment adheres to the same procedure outlined in Section 4.

S1. Success Rate by Language Model and Task

Success rates for each spatial challenge are displayed by language model in Figure 8. The LLM+DL framework significantly increases success rates compared to LLM-only control in almost all configurations, while absolute performance differs among models.

S2. Average Steps by Language Model

Figure 9 provides an additional analysis of efficiency by breaking down the average number of steps needed for successful episodes by task and language model. While LLM+DL consistently converges faster across all models, the LLM-only control shows substantial volatility and noticeably increased step counts.

S3. Convergence Behavior Across Tasks

Normalized distance-to-goal curves for each of the four spatial relations are shown in Figure 10. These figures show that while the LLM+DL framework generates smooth, monotonic trajectories with lower variance, LLM-only control frequently displays oscillatory or non-monotonic convergence.

S4. Model-Specific Relative Improvements

Figure 11 shows the speedup factors and success-rate increases of LLM+DL over LLM-only control for each language model in order to measure the advantage of neuro-symbolic integration at the model level.

S5. Discussion of Supplementary Results

The additional findings support the paper’s primary conclusions. In every in-depth analysis, the LLM+DL framework shows:

- Gains in performance that are consistent across different-scale language models
- Considerable decreases in convergence time and control steps
- Reduced variation and increased stability in closed-loop behavior

The efficacy of clearly distinguishing symbolic reasoning from continuous execution in language-conditioned control tasks is further supported by these results.

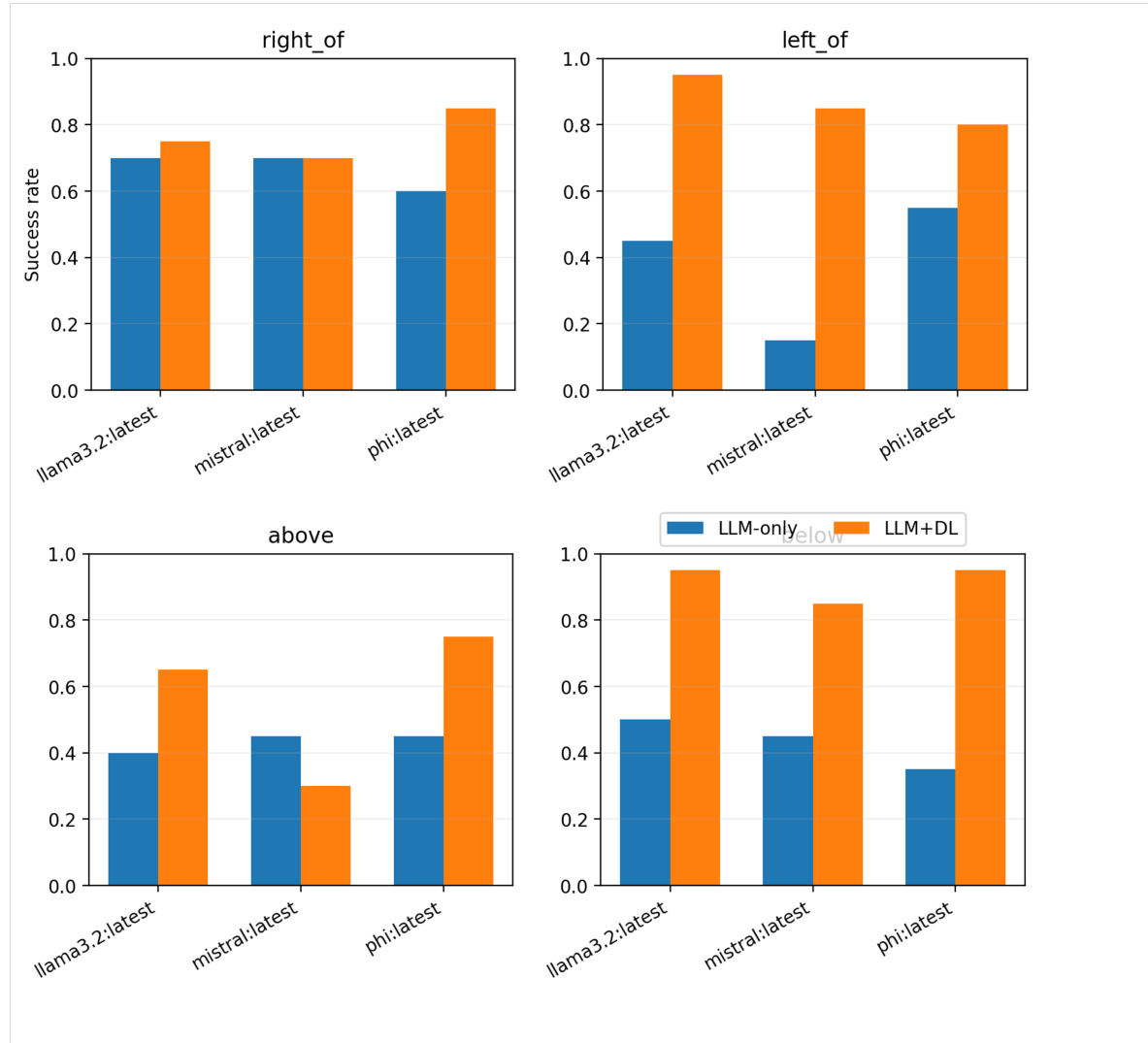


Figure 8: Success rate by task and language model. The neuro-symbolic LLM+DL framework improves reliability across all evaluated LLMs, including smaller models such as Phi.

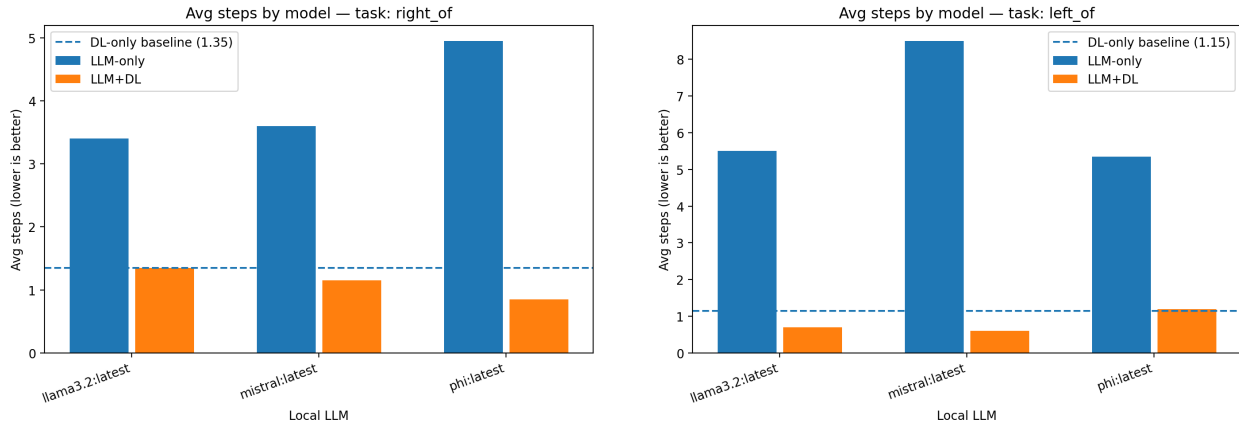


Figure 9: The average number of control steps for the left_of and right_of tasks by language model. For all models, LLM+DL achieves significant step count reductions.

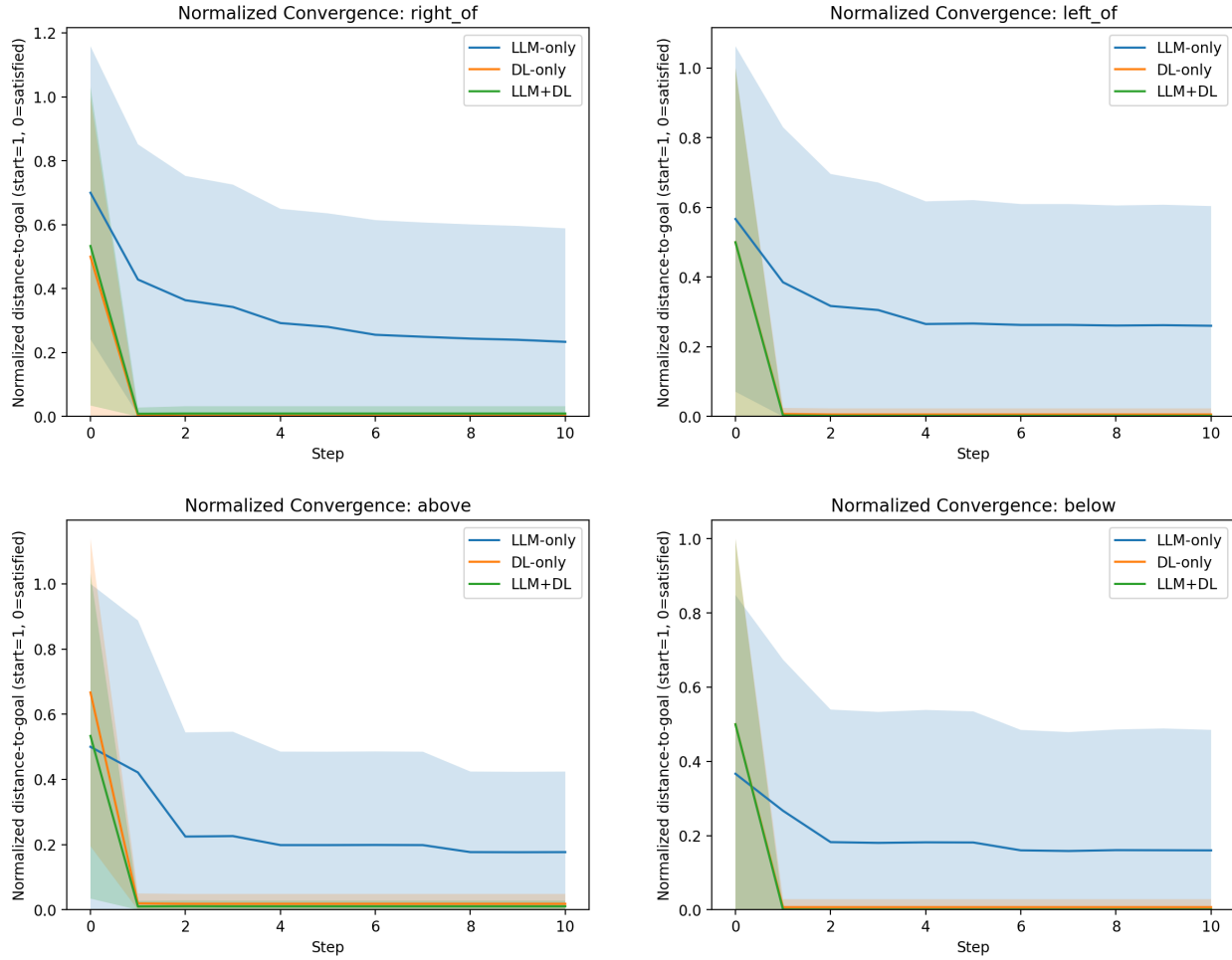


Figure 10: Normalized distance-to-goal over time for all spatial tasks. The proposed LLM+DL framework converges faster and more stably than LLM-only control across all relations.

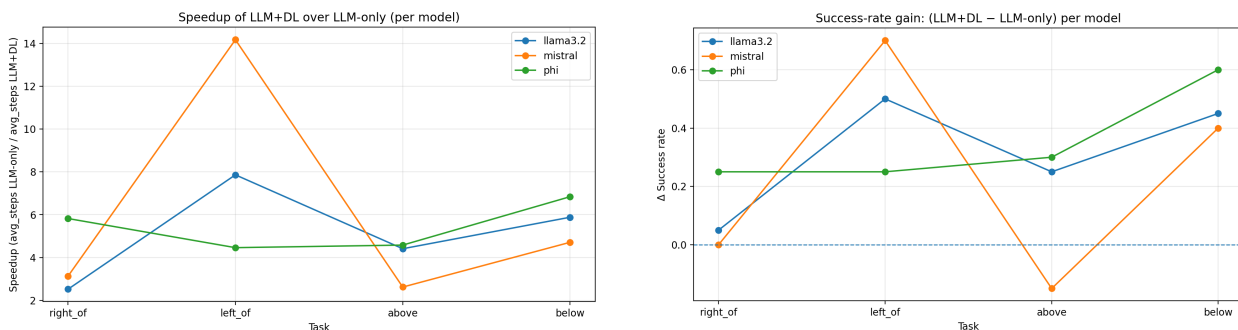


Figure 11: Model-specific speedup (left) and success-rate improvement (right) of LLM+DL over LLM-only control. Performance gains are consistent across all evaluated language models.